Supporting Information

Nanoscale Electrocatalysis: Visualizing Oxygen Reduction at Pristine, Kinked and Oxidized Sites on Individual Carbon Nanotubes

Joshua C. Byers, Aleix G. Güell, Patrick R. Unwin*

Department of Chemistry, University of Warwick, Gibbet Hill Road, Coventry, CV4 7AL, U.K.

*Corresponding author: p.r.unwin@warwick.ac.uk

Index *Page*

Section 1. Growth of single walled carbon nanotubes via chemical vapor deposition

Single walled carbon nanotubes (SWNTs) were grown using catalyzed chemical vapor deposition (cCVD) onto oxidised Si wafers (IDB Technologies Ltd., n-type Si, 525 μm thickness, 300 nm oxide). Ferritin Type 1 solution (from horse spleen, Sigma Aldrich) was diluted (1:200) into deionized water (18.2 MΩ, Purite) and used as a catalyst source for SWNT growth.[1,2] Square sections of oxidized Si wafer (2.5 cm x 2.5 cm) were cleaned with isopropanol and dipped (5 mm depth) into ferritin solution for 20 minutes forming a thin film along one of the edges of the substrate.[1,3] The substrates were blown dry using nitrogen gas (direction away from the uncoated region) and ashed in an oxygen plasma using a K1050X Plasma Etcher/Asher/Cleaner (Emitech, UK) at 100 W for 2 minutes.

A custom-built cold wall CVD system (Moorfields, UK) was used for growth of millimeter long flow-aligned SWNTs. Following nanotube growth, a Pd contact (~70 nm thick) was made to the SWNTs using thermal evaporation (Moorfields, UK). A 2 nm Cr adhesion layer was thermally evaporated prior to Pd deposition. The metal films were deposited on the area where the catalyst layer resided, being defined by a stencil shadow mask. No further processing was required, ensuring minimal manipulation and perturbation of the SWNTs. Example images, field emission – scanning electron microscopy (FE-SEM) (ZEISS SUPRA-55VP), of a well-aligned SWNT and one containing a kinked region are shown in Figure S1.

Subsequently, a section of the SWNT approximately 200 μm away from the metal contact, was decorated with silver particles by means of electrodeposition[3,4] allowing the localization of the nanotube by optical microscopy (for further interrogation with complementary techniques). The Ag particle ensemble delineated a section of the SWNT between the metal contact and the silver particles. In-depth details of this type of *individualized* flow-aligned SWNT experiment (SWNT synthesis, sample preparation and characterization) can be found elsewhere.[3]

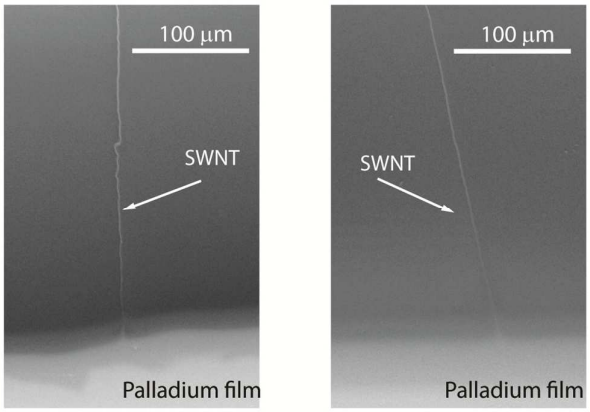

Figure S1. FE-SEM images of a SWNT containing a kink region (left image) and a well-aligned SWNT (right image), contacted by Pd metal contact pads.

Section 2. Scanning electrochemical cell microscopy (SECCM) set-up

Nanoscale electrochemical imaging using SECCM was realized by translating a theta capillary in the x-y-z directions over the substrate surface with nanometer control as illustrated in Figure 1a of the main text. Coarse positioning of the pipet was achieved using micro-positioners (M-461, Newport). Fine control of the pipet, electrochemical potential, and data acquisition were done using an FPGA card (PCIe-7852R, National Instruments) controlled using a Labview interface (program written by Dr. K. McKelvey). Nanopositioning of the pipet perpendicular to the surface utilized a linear actuator (P-753, PI) and controller (E665, PI), and laterally using x-y stages (P-621, PI) and controllers (E625, PI) for the plane of the substrate.

A borosilicate glass theta pipet (TGC150-10, Harvard Apparatus) was pulled to sub-micron size (measured precisely using FE-SEM, vide infra) using a CO2 laser puller (P-2000, Sutter Instruments). Each of the barrels in the pipet was filled with a phosphate buffer solution (pH 7.2, Fluka) and 25 mM KCl, resulting in a meniscus at the tapered pipet end. Chloridized

silver wires were inserted into each barrel to act as quasi-reference counter electrodes (QRCEs). Ag/AgCl QRCEs were found to have a potential of + 0.0965 V versus a standard Ag/AgCl (3M KCl) reference electrode in the phosphate buffer solution (pH 7.2) and 25 mM KCl. A constant offset voltage (V_2 in main text Figure 1a) was applied to one of the QRCEs that led to a dc ion current (I_{IC} in main text Figure 1a) between the two barrels. A small amplitude oscillation of the pipet perpendicular to the surface (40 nm peak-to-peak) induced an additional ac ion current between the two barrels. The oscillation frequency was generated and detected using a lock-in amplifier (SR380, Stanford Research Systems) and the resulting ac ion current served as a feedback signal to maintain a constant tip-substrate separation as the pipet was translated across the substrate surface. The working electrode potential was controlled by V_1 (main text Figure 1a) and an electrochemical current (I_{EC}) was measured by a custom-built high sensitivity current-to-voltage converter, when the meniscus made contact with the SWNT. Further details can be found in.[5,6] Scan rates of 0.5 – 1 μm s^{-1} were used to acquire all of the maps.

Section 3. Raman spectroscopy

Micro-Raman spectroscopy (Argon 514 nm laser, 10 mW, 50x lens, NA 0.85, inVia micro-Raman, Renishaw, UK) was used to determine the nature of the SWNT. The signals in the G-band region, around 1580 cm^{-1} corresponding to the tangential mode of the SWNTs, and the radial breathing mode (RBM) region between 100 and 300 cm^{-1} were used to characterize the SWNTs. As an example, Figure S2 shows the Raman spectrum for the SWNT used to record Figure 1b of the main text. The G-band exhibits one peak at 1590 cm^{-1} (G+) and another broader and asymmetric peak with a Breit-Wigner-Fano lineshape, at lower frequency (G-)[7,8] confirming the metallic nature of the nanotube. A well-defined RBM peak (182 cm^{-1}) was observed at lower frequencies to confirm the single-walled character of the nanotube and to

determine its diameter, since the RBM frequency, ω_{RBM}, and SWNT diameter, d_{SWNT}, are related through:[9]

$$\omega_{RBM} = \frac{A}{d_t} \qquad \text{(S1)}$$

where A = 248 cm^{-1}. This equation is valid for an individual SWNT on a silicon oxide substrate[9] and has been proven against AFM data.[3] The resulting SWNT diameter was ~ 1.4 nm, consistent with the typical dimensions obtained for this type of SWNT growth.[1,3]

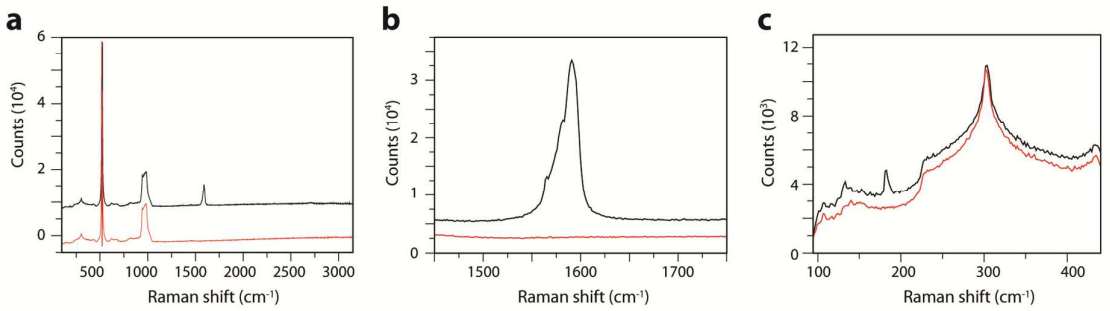

Figure S2. (a) Raman survey spectra of a SWNT (black line) compared with bare silicon/silicon oxide substrate (red line). (b) Spectra of the G-band region. (c) Spectra of the radial breathing mode region.

Section 4. Oxygen reduction on HOPG

Comparison measurements were made of the ORR on freshly cleaved HOPG (high quality, ungraded material original from Dr. Arthur Moore, Union Carbide, and kindly provided by Prof. R.L. McCreery, University of Alberta, Canada). A typical voltammogram is shown in Figure S3. A limiting current of ca. 120 pA, assigned to a two electron reduction, can just be discerned before the onset of water reduction. This material has been extremely well characterized and shown to have a low step density.[10]

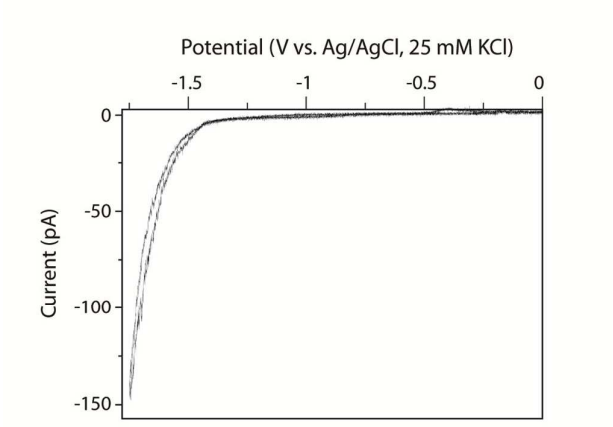

Figure S3. Cyclic voltammogram for the ORR of HOPG measured in 25 mM KCl in phosphate buffer solution (pH 7.2) using Ag/AgCl QRCEs. Scan rate: 100 mV s^{-1}.

Section 5. Complementary SECCM maps: *dc*, *ac* and *z*-displacement

In addition to measuring the electrochemical current during substrate mapping, SECCM records the *dc* ion current, *ac* ion current and *z*-piezo displacement simultaneously, providing a set of complementary maps that offer insight into the meniscus size (meniscus stability), tip-substrate separation and substrate surface features during imaging. The tip-substrate separation is assumed to be defined by the hemispherical droplet formed at the end of the pipette, which for a pipette diameter of 500 nm gives a separation of 250 nm. Complementary maps were acquired simultaneously with the electrochemical map to confirm the meniscus footprint and droplet stability. A set of complementary maps are shown in Figure S4 to illustrate the consistency of the experimental set-up throughout the measurement. These maps correspond to the measurement of Figure 3b of the main text, where the greatest enhancement of electrochemical activity was observed, and where changes to meniscus size would be expected to have the most pronounced effect. Similar maps were obtained for all electrochemical images. There is little variation in these quantities (< 10 %) over the entire scanned area which is predominantly the silicon oxide substrate and even less variation along the SWNT. The *dc* ion current map indicates that the meniscus volume is constant throughout the measurement process, which is consistent with the constant tip-substrate separation in the *ac* ion current map. There is some tilt evident in the z-displacement (as found generally in scanned probe microscopy topography images), however, this has little impact on the meniscus size or tip-substrate separation as confirmed in the supporting *ac* and *dc* ion current maps.

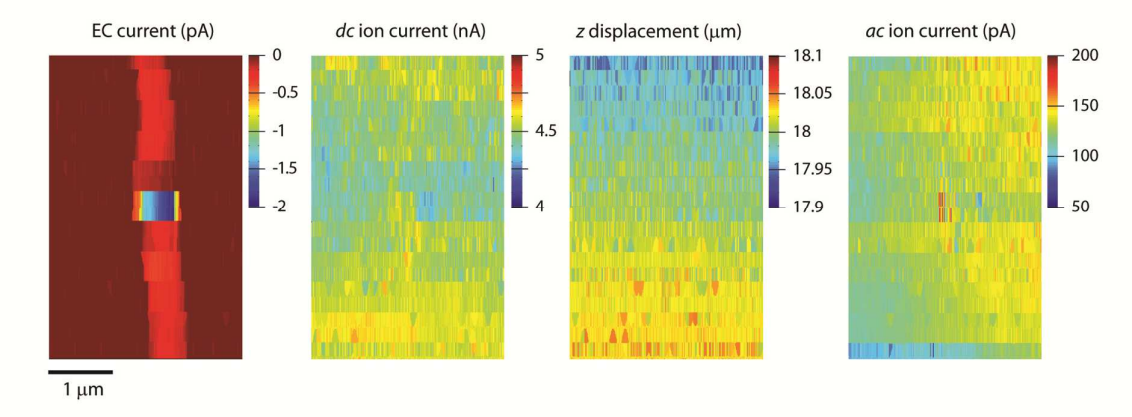

Figure S4. Set of complementary maps of a SWNT (corresponding to in Figure 3b of the main text) obtained with SECCM: electrochemical current (I_{EC}), *dc* ion current, *z*-piezo displacement and *ac* ion current.

Section 6. Tafel Analysis

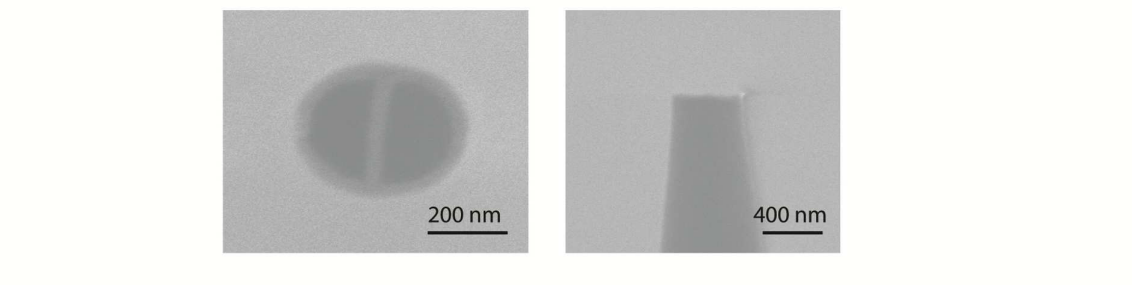

Figure S5. FE-SEM image of a complementary theta pipet used for imaging showing the tip opening (left image) and side profile (right image).

The diffusion current density, j_d, for the pristine and oxidized SWNT were - 4.19 A cm^{-2} and - 1.9 A cm^{-2} respectively determined using the electrode geometry defined in the main text. The kinetic current density was calculated using equation (4) of the main text, which closely followed the current densities of the voltammograms over the potential region used for Tafel analysis as a consequence of the high mass transport rates obtained using SECCM.

To enable comparison with other studies, j^o was normalized by the bulk concentration of oxygen (2.5×10^{-7} mol cm^{-3}) for the measurements made in aerated solution using SECCM.[11] The value used for the oxygen concentration[12-14] for the polycrystalline Au and Au/C samples was 1.26×10^{-6} mol cm^{-3}. To determine the overpotential, η, the potential of chloridized Ag wire QRCEs was measured in the same solution used for the measurements in this work (25 mM KCl in phosphate buffer solution, pH 7.2) versus a known reference electrode Ag/AgCl (3M KCl). The potential of Ag/AgCl (3M KCl) is + 0.222 V vs. NHE at pH = 0. The measured potential of the QRCE vs. Ag/AgCl (3 M KCl) reference electrode was + 0.0965 V, giving $E_{QRCE\ vs.\ NHE\ (pH\ 0)}$ = + 0.318 V.The standard electrode potential for oxygen reduction to hydrogen peroxide at pH 14 is - 0.133 V vs. NHE, as given in equation 1, of the main text.[15] The measurements in this work were carried out at a pH of 7.2 and there is a shift in potential of 59 mV per pH unit, so that $E_{QRCE\ vs.\ NHE\ (pH\ 7.2)}$ = + 0.0478 V.

References

(1) Güell, A. G.; Ebejer, N.; Snowden, M. E.; McKelvey, K.; Macpherson, J. V.; Unwin, P. R. *Proc. Natl. Acad. Sci. U. S. A.* **2012**, *109*, 11487.

(2) Li, Y.; Kim, W.; Zhang, Y.; Rolandi, M.; Wang, D.; Dai, H. *J. Phys. Chem. B* **2001**, *105*, 11424.

(3) Güell, A. G.; Meadows, K. E.; Dudin, P. V.; Ebejer, N.; Macpherson, J. V.; Unwin, P. R. *Nano Lett.* **2014**, *14*, 220.

(4) Dudin, P. V.; Snowden, M. E.; Macpherson, J. V.; Unwin, P. R. *ACS Nano* **2011**, *5*, 10017.

(5) Ebejer, N.; Güell, A. G.; Lai, S. C. S.; McKelvey, K.; Snowden, M. E.; Unwin, P. R. *Annu. Rev. Anal. Chem.* **2013**, *6*, 329.

(6) Snowden, M. E.; Güell, A. G.; Lai, S. C. S.; McKelvey, K.; Ebejer, N.; O'Connell, M. A.; Colburn, A. W.; Unwin, P. R. *Anal. Chem.* **2012**, *84*, 2483.

(7) Jorio, A.; Souza, A. G.; Dresselhaus, G.; Dresselhaus, M. S.; Swan, A. K.; Unlu, M. S.; Goldberg, B. B.; Pimenta, M. A.; Hafner, J. H.; Lieber, C. M.; Saito, R. *Phys. Rev. B* **2002**, *65*, 9.

(8) Brown, S. D. M.; Jorio, A.; Corio, P.; Dresselhaus, M. S.; Dresselhaus, G.; Saito, R.; Kneipp, K. *Phys. Rev. B* **2001**, *63*, 8.

(9) Dresselhaus, M. S.; Dresselhaus, G.; Saito, R.; Jorio, A. *Phys. Rep.-Rev. Sec. Phys. Lett.* **2005**, *409*, 47.

(10) Patel, A. N.; Collignon, M. G.; O'Connell, M. A.; Hung, W. O. Y.; McKelvey, K.; Macpherson, J. V.; Unwin, P. R. *J. Am. Chem. Soc.* **2012**, *134*, 20117.

(11) Slevin, C. J.; Ryley, S.; Walton, D. J.; Unwin, P. R. *Langmuir* **1998**, *14*, 5331.

(12) Jirkovsky, J. S.; Halasa, M.; Schiffrin, D. J. *Phys. Chem. Chem. Phys.* **2010**, *12*, 8042.

(13) Jirkovský, J. S.; Panas, I.; Ahlberg, E.; Halasa, M.; Romani, S.; Schiffrin, D. J. *J. Am. Chem. Soc.* **2011**, *133*, 19432.

(14) Siahrostami, S.; Verdaguer-Casadevall, A.; Karamad, M.; Deiana, D.; Malacrida, P.; Wickman, B.; Escudero-Escribano, M.; Paoli, E. A.; Frydendal, R.; Hansen, T. W.; Chorkendorff, I.; Stephens, I. E. L.; Rossmeisl, J. *Nat. Mater.* **2013**, *12*, 1137.

(15) Yeager, E. *Electrochim. Acta* **1984**, *29*, 1527.